

# Geometrical scaling of heavy-quark contributions in the low $x$ region

G.R.Boroun\*

*Department of Physics, Razi University, Kermanshah 67149, Iran*  
(Dated: April 19, 2022)

We describe the determination of the heavy quarks structure functions  $F_{2,L}^{\mathcal{Q}\overline{\mathcal{Q}}}$  with help of the scaling properties. We observe that the structure functions for inclusive charm and bottom production exhibits geometric scaling at low  $x$ . The geometrical scaling means that the heavy quark structure function is a function of only one dimensionless variable  $\tau \equiv Q^2/Q_{sat}^2(x)$  including quark mass. These results are valid for any value of  $\delta$ , being  $x^{-\delta}$  the behavior of the parton densities at low  $x$ . The determination of the heavy quark structure function is presented as a parameterization of the proton structure function  $F_2(x, Q^2)$  and its derivative. Analytical expressions for  $F_{2,L}^{\mathcal{Q}\overline{\mathcal{Q}}}$  in terms of the effective parameters of the parameterization of  $F_2(x, Q^2)$ , with respect to the BDH and ASW models, are presented. To study the heavy quark production processes, we use the collinear results in DAS approach. Numerical calculations and comparison with HERA data demonstrate that the suggested method provides reliable  $F_{2,L}^{\mathcal{Q}\overline{\mathcal{Q}}}$ ,  $R^{c\overline{c}}$  and  $\sigma^{\mathcal{Q}\overline{\mathcal{Q}}}$  at low  $x$  in a wide range of the low absolute four-momentum transfers squared ( $4 \text{ GeV}^2 < Q^2 < 2000 \text{ GeV}^2$ ). Also, in the HERA kinematic range, the ratio of  $F_2^{c\overline{c}}/F_2$ ,  $F_2^{b\overline{b}}/F_2^{BDHM}$  and  $F_2^{b\overline{b}}/F_2^{BDHM}$  are obtained. Expanding the method to low and ultra low values of  $x$  can be considered in the process analysis of the LHeC and FCC-eh colliders.

## 1. INTRODUCTION

In earlier HERA experiments, data on charm and bottom structure functions,  $F_2^{c\overline{c}}(x, Q^2)$  and  $F_2^{b\overline{b}}(x, Q^2)$ , were found to be around %25 and %1 of the proton structure function  $F_2(x, Q^2)$  at small  $x$  respectively. In ultrahigh energy processes, at extremely small  $x$ , these percents will be increased and checked in high energy processes such as the Large Hadron electron Collider (LHeC) and the Future Circular Collider electron-hadron (FCC-eh) projects which run to beyond a TeV in center-of-mass energy [1]. These new colliders lead into the region of high parton densities at low  $x$  as the kinematic reach of maximum  $Q^2 \sim 1 \text{ TeV}^2$  and  $x \sim 10^{-5} \dots 10^{-6}$  for LHeC and  $10^{-7}$  for FCC-eh. By electron-proton (ep) colliders, the heavy quarks can be produced in pair in the deep inelastic scattering (DIS) through neutral current (NC) production. In these regions, the gluon density becomes predominant and the heavy quarks behavior will be checked in the photo-gluon fusion reactions. The production of heavy quarks at HERA depend on the mass of these quarks and thus the calculations of cross sections depend on a wide range of perturbative scales  $\mu^2$ . The first production of heavy quarks at HERA is keeping by fixed number of parton densities (fixed flavour number schemes, FFNS) close to threshold  $\mu^2 \sim m_{\mathcal{Q}}^2$  (where  $m_{\mathcal{Q}}$  is the heavy quark mass), as

$$F_{2,L}^{\mathcal{Q}\overline{\mathcal{Q}}} |_{\text{FFNS}} = \sum_{j=0}^{\infty} a_s^j(n_f) \sum_{i=q,g} H_{k,i}^{(j)}(n_f) \otimes f_i(n_f), \quad (1)$$

where  $H$ 's are the Wilson coefficients for the DIS heavy-quark production [2] and the dynamics of flavor-singlet quark and gluon distribution functions,  $q^s$  and  $g$ , are defined by

$$\begin{aligned} q^s(x, n_f, \mu^2) &= \sum_{l=1}^{n_f} [f_l(x, n_f, \mu^2) + \overline{f}_l(x, n_f, \mu^2)], \\ g(x, n_f, \mu^2) &= f_g(x, n_f, \mu^2), \end{aligned} \quad (2)$$

where  $n_f$  is the number of active quark flavors. FFNS can be used on the threshold of  $\mu^2 \sim m_{\mathcal{Q}}^2$  and for  $\mu^2 > m_{\mathcal{Q}}^2$  the variable-flavour-number scheme (VFNS) is used where the treatment of resummation of collinear logarithms  $\ln(\mu^2/m_{\mathcal{Q}}^2)$  is achieved. For realistic kinematics it has to be extended to the case of a general-mass VFNS (GM-VFNS) which is defined similarly to the zero-mass VFNS (ZM-VFNS) in the  $Q^2/m_{\mathcal{Q}}^2$  limit [3-6]. The heavy-quark structure functions derived using the zero-mass VFNS scheme (ZM-VFNS) as

$$\begin{aligned} F_{2,L}^{\mathcal{Q}\overline{\mathcal{Q}}} |_{\text{ZM-VFNS}} &= \sum_{j=0}^{\infty} a_s^j(n_f+1) \sum_{i=q,g,\mathcal{Q}} C_{k,i}^{(j)}(n_f+1) \\ &\otimes f_i(n_f+1), \end{aligned} \quad (3)$$

where  $C$ 's are the Wilson coefficients at the  $j$ -th order and  $a_s = \frac{\alpha_s}{4\pi}$  is the QCD running coupling. For  $Q^2 \sim m_{\mathcal{Q}}^2$  VFNS is valid where it includes a combination of the ZM-VFNS with FFNS.

The heavy-quark structure functions obtained in DIS at HERA, from the measurement of the inclusive heavy quark cross sections, are an important test of the QCD [7]. The heavy-quark reduced cross section defined in terms of the heavy-quark structure functions as

$$\sigma_{\text{red}}^{\mathcal{Q}\overline{\mathcal{Q}}}(x, Q^2) = F_2^{\mathcal{Q}\overline{\mathcal{Q}}}(x, Q^2) - f(y) F_L^{\mathcal{Q}\overline{\mathcal{Q}}}(x, Q^2), \quad (4)$$

\*Electronic address: boroun@razi.ac.ir

where  $f(y) = \frac{y^2}{1+(1-y)^2}$  and  $y = Q^2/sx$  is the inelasticity with  $s$  the ep center of mass energy squared. In HERA kinematic range the contribution  $F_L^{\mathcal{Q}\overline{\mathcal{Q}}}$  is small, therefore the heavy-quark structure function  $F_2^{\mathcal{Q}\overline{\mathcal{Q}}}$  is obtained from the measured heavy-quark cross section. Future circular colliders (LHeC and FCC-he) will extend the ratio  $F_L^{\mathcal{Q}\overline{\mathcal{Q}}}/F_2^{\mathcal{Q}\overline{\mathcal{Q}}}$  into a region of much smaller  $x$  and higher  $Q^2$ . Indeed these new colliders are the ideal place to resolve this ratio [1].

In deep inelastic scattering (DIS), the photon-proton cross section for heavy-quark production is related to the heavy-quark structure function with the following form

$$\sigma^{\mathcal{Q}\overline{\mathcal{Q}}}(x, Q^2) = 4\pi^2\alpha_{em}F_2^{\mathcal{Q}\overline{\mathcal{Q}}}(x, Q^2)/Q^2. \quad (5)$$

One of the well-known property of deep inelastic scattering at low  $x$  is geometrical scaling (GS) [8-10]. GS is the statement that the  $\sigma^{\mathcal{Q}\overline{\mathcal{Q}}}(x, Q^2)$ , which is a priori function of two independent variables  $(x, Q^2)$ , depends only on a specific combination of them,  $\tau = Q^2/Q_s^2(x)$ , where function  $Q_s(x)$  called saturation scale. In principle  $\sigma^{\mathcal{Q}\overline{\mathcal{Q}}}(x, Q^2) = \sigma^{\mathcal{Q}\overline{\mathcal{Q}}}(\tau)$ . The saturation scale is a border between dense and dilute gluonic systems where was taken in the following form

$$Q_s^2(x) = Q_0^2(x/x_0)^{-\lambda} \quad (6)$$

Here  $Q_0 = 1$  GeV and the parameters  $x_0$  and  $\lambda$  were determined from a fit to DIS data at low  $x$  [11]. The gluon saturation appears formally due to the nonlinearities of parton evolution at low  $x$  given by JIMWLK equations [12]. A description of this low  $x$  regime is given by the Color Glass Condensate (CGC), a semi-classical effective field theory (EFT) for low  $x$  gluons. In this model the transition between the color transparency and the dipole correlator is delineated by defining the saturation scale  $Q_s(x)$ . These two regimes are defined into small separations  $r_\perp$  and large distances  $r_\perp$  respectively, where  $r_\perp$  is the dipole separation [13-14].

In heavy quarks production GS is expected to be violated due to large quarks mass. To do this we replace the Bjorken scaling by the rescaled variable

$$\chi = x(1 + \frac{4m_{\mathcal{Q}}^2}{Q^2}) = \frac{Q^2 + 4m_{\mathcal{Q}}^2}{W^2} \quad (7)$$

and keep  $m_{\mathcal{Q}} \neq 0$ . Here  $W$  is the total energy of the  $\gamma^*p$  system. The rescaling variable is one of the ingredients used in the GM-VFNS. The cross section for heavy quark pair production vanishes when  $\chi$  goes to 1 for  $W$  as small as  $2m_{\mathcal{Q}}$  [15]. Main purpose of this paper is to asses the GS in heavy quark pair production. To this end we take into account  $m_{\mathcal{Q}}$  in

$$\tau = Q^2/Q_0^2(1 + \frac{4m_{\mathcal{Q}}^2}{Q^2})^\lambda(x/x_0)^\lambda, \quad (8)$$

to H1 and ZEUS data [16] on charm and bottom structure functions.

In the present paper we present a method of extraction of the heavy quark structure functions,  $F_2^{\mathcal{Q}\overline{\mathcal{Q}}}(x, Q^2)$  and  $F_L^{\mathcal{Q}\overline{\mathcal{Q}}}(x, Q^2)$  in the kinematical region of low values of the Bjorken variable  $x$  from the parameterization models by relying on the saturation scaling arguments. Indeed a simple parametrization for the heavy quark structure function in the region of  $x < 0.1$  in a wide interval of photon virtualities is proposed. The organization of this paper is as follows. In section II we introduce the basic formula used for the definition of evolution equations and color dipole picture. In section III we present the heavy quark structure functions with respect to the proton parameterization models. The main results and finding of the present heavy quark structure functions due to the modified geometrical scaling is discussed in detail in section IV. In the same section, the feasibility of measuring  $F_2^{\mathcal{Q}\overline{\mathcal{Q}}}(x, Q^2)$ , in the available energy to the range of new collider energies (i.e., LHeC and FCC-he), is investigated. Conclusions and summary are summarized on Sec.V.

## 2. Deep-inelastic Structure Functions

Measurements at HERA have shown that heavy flavor production in DIS proceeds predominantly via the photon-gluon fusion process  $\gamma g \rightarrow \mathcal{Q}\overline{\mathcal{Q}}$ , as the reaction under study is

$$e^- + P \rightarrow e^- + \mathcal{Q}\overline{\mathcal{Q}} + X, \quad (9)$$

where  $P$  is a proton,  $\mathcal{Q}\overline{\mathcal{Q}}$  is a pair heavy-quark and  $X$  is any hadronic state allowed. The differential cross section  $\sigma^{\mathcal{Q}\overline{\mathcal{Q}}}$  (hereafter  $\mathcal{Q} = c, b$ ) can be presented in the following form

$$\begin{aligned} \frac{d^2\sigma^{\mathcal{Q}\overline{\mathcal{Q}}}}{dx dQ^2} &= \frac{2\pi\alpha^2}{xQ^4} [(1 + (1-y)^2)F_2^{\mathcal{Q}\overline{\mathcal{Q}}}(x, Q^2) \\ &\quad - \frac{y^2}{2}F_L^{\mathcal{Q}\overline{\mathcal{Q}}}(x, Q^2)], \end{aligned} \quad (10)$$

where  $F_k^{\mathcal{Q}\overline{\mathcal{Q}}}(x, Q^2)$  (hereafter  $k = 2, L$ ) is heavy quark parts of the proton structure function  $F_k(x, Q^2)$  [17,18]. Analogous studies have been performed in Ref.[18] which is based on the transverse momentum dependent (TMD) gluon density. TMD, or non-integrated, functions depending on the fraction of the longitudinal momentum  $x$  of the proton carried by the parton, the two-dimensional transverse momentum of the parton  $\mathbf{K}_T^2$ , and the hard scale  $\mu^2$  of a complex process, contain nonperturbative information about the proton structure, including the transverse momentum.

In the small  $x$  region, the heavy quark structure functions in the collinear generalized double asymptotic scaling (DAS) approach are given by [18]

$$F_k^{\mathcal{Q}\overline{\mathcal{Q}}}(x, Q^2) = C_{k,g}(x, Q^2, m_Q^2) \otimes f_g(x, \mu^2), \quad (11)$$

where  $C_{k,g}(x, Q^2)$  are the Wilson coefficient functions and  $\mu$  is the renormalization scale. The symbol  $\otimes$  is the Mellin convolution

$$F_k^{\mathcal{Q}\overline{\mathcal{Q}}}(x, Q^2) = \int_x^{x_2} \frac{dy}{y} C_{k,g}(y, \xi) f_g\left(\frac{x}{y}, \mu^2\right), \quad (12)$$

where  $x_2 = 1/(1 + 4\xi)$ ,  $\xi = m_Q^2/Q^2$  and  $f_g(x, Q^2)$  is the gluon density. The renormalization and factorization scales were set to be equal to  $\mu_R^2 = 4m_Q^2 + Q^2$  and  $\mu_F^2 = Q^2$ , respectively [19,20]. The coefficient functions at leading order (LO) up to next-to-next-to leading order (NNLO) approximations are defined [18,21]

$$C_{k,g}(x, a_s) = e_Q^2 \sum_{n=0} (a_s(\mu^2))^{n+1} B_{k,g}^{(n)}(x, \xi), \quad (13)$$

where in the high energy regime the coefficients  $B_{k,g}^{(n)}(x, \xi)$  have the compact forms defined in literature and  $n$  denotes the order in running coupling  $\alpha_s(\mu^2)$  [18-21].

Using the fact that the non-singlet contribution can be ignored safely at low values of  $x$ . According to the famous DGLAP equations, the evolution of the singlet structure function reads

$$\begin{aligned} \frac{\partial F_2(x, Q^2)}{\partial \ln Q^2} &= -\frac{1}{2} \sum_{n=0} (a_s(Q^2))^{n+1} [\tilde{P}_{ss}^{(n)}(x) \otimes F_2(x, Q^2) \\ &+ \langle e^2 \rangle \tilde{P}_{sg}^{(n)}(x) \otimes x f_g(x, Q^2)], \end{aligned} \quad (14)$$

where

$$\begin{aligned} \tilde{P}_{ab}^{(0)}(x) &= P_{ab}^{(0)}(x), \\ \tilde{P}_{ab}^{(n)}(x) &= P_{ab}^{(n)}(x) + \sum_m B_{2,b}^{(n)}(x) \otimes P_{ab}^{(n-1)}(x) \\ &+ 2\beta_0 \sum_m B_{2,b}^{(n)}(x) \otimes \delta(1-x) + \dots, \quad n > 0 \end{aligned}$$

The quantities  $\tilde{P}_{ab}$ 's are expressed via the known splitting and Wilson coefficient functions in literatures and  $P_{ab}$  are the splitting functions in [18-21]. In the above equation  $\langle e^k \rangle$  is the average of the charge  $e^k$  for the active quark flavors,  $\langle e^k \rangle = n_f^{-1} \sum_{i=1}^{n_f} e_i^k$ .

Parametrization of the proton structure function suggested in Ref.[22] by M.M.Block, L.Durand and P.Ha, in what follows referred to as the MDH model (BDHM), describe fairly well the available experimental data on the reduced cross sections and, at asymptotically low  $x$ , provide a behavior of the cross sections  $\sim \ln^2 1/x$ , in an agreement with the Froissart predictions. This suggested method provides reliable proton structure functions  $F_2(x, Q^2)$  with  $x \leq 0.1$  in a wide range of the momentum transfer ( $0.15 \text{ GeV}^2 < Q^2 < 3000 \text{ GeV}^2$ ) and

can be applied as well in analyses of ultrahigh energy processes with cosmic neutrinos. The explicit expression for the BDHM reads

$$F_2^{\text{BDH}}(x, Q^2) = D(Q^2)(1-x)^\nu \sum_{m=0}^2 A_m(Q^2) L^m, \quad (15)$$

where the effective parameters are defined in Refs.[22,23]. In the framework of color glass condensate an analytic proton structure function including quark mass has suggested by authors in Ref.[24]. Those kept the quark mass in photon wave function and obtained the massive proton structure function. The proton structure function in the dipole frame, obtained via

$$F_2(x, Q^2) = \frac{Q^2}{4\pi^2\alpha} [\sigma_L^{\gamma^*p}(x, Q^2) + \sigma_T^{\gamma^*p}(x, Q^2)] \quad (16)$$

where the subscripts  $L$  and  $T$  denote the longitudinal and transverse polarizations of the virtual photon. In this frame the photon undergoes the hadronic interaction through dissociation of the photon into a quark-antiquark ( $q\bar{q}$ ) pair of flavor  $f$  and size  $r$ , called dipole, and the interaction of the quark-antiquark pair with the target proton [25]. Within the dipole framework of the  $\gamma^*p$  scattering the photoabsorption cross section is written as

$$\sigma_{L,T}^{\gamma^*p}(x, Q^2) = \int d^2\mathbf{r} \int dz \psi^*(Q, r, z) \hat{\sigma}(x, r) \psi(Q, r, z) \quad (17)$$

Here the quark (or antiquark) carries a fraction  $z$  of the incoming photon light-cone energy ( $0 < z < 1$ ). The wave function squared of the  $q\bar{q}$  Fock states of the virtual photon is given by the following equations

$$\begin{aligned} |\Psi_T(z, r)|^2 &= \frac{6\alpha_{em}}{4\pi^2} \sum_1^{n_f} e_f^2 \{ [z^2 + (1-z)^2] \epsilon^2 K_1^2(\epsilon r) \\ &+ m_f^2 K_1^2(\epsilon r) \}, \end{aligned}$$

and

$$|\Psi_L(z, r)|^2 = \frac{6\alpha_{em}}{4\pi^2} \sum_1^{n_f} e_f^2 \{ 4Q^2 z^2 (1-z)^2 K_0^2(\epsilon r) \} \quad (18)$$

where  $\epsilon^2 = z(1-z)Q^2 + m_f^2$  and  $m_f$  is the quark mass.  $e_f$  is the quark charge and the functions  $K_{0,1}$  are the Bessel-McDonald functions. With respect to the GBW model [11] inspired by geometrical scaling, the dipole cross-section is defined by

$$\sigma_{\text{dipole}}(x, Q^2) = \sigma_0 \{ 1 - \exp(-\frac{r^2 Q_s^2(x)}{4}) \}. \quad (19)$$

Authors in Ref.[24] defined the cross-section of  $\gamma^*p$  scattering by the following form

$$\begin{aligned} \sigma_{L,T}^{\gamma^*p}(x, Q^2) &= -\sigma_0 \int \mathcal{F}_{L,T}(\zeta, \frac{m_f^2}{Q^2}) [\frac{Q_0^2}{Q^2} (\frac{x}{x_0})^{-\lambda}]^{1/2+i\zeta} \\ &\times \Gamma(-\frac{1}{2} - i\zeta) \frac{d\zeta}{2\pi} \end{aligned} \quad (20)$$

Therefore the massive analytic proton structure function reads

$$F_2(x, Q^2) = \frac{Q^2}{4\pi^2\alpha} \sigma'_0 \left\{ \ln \left[ \left( \frac{x_0}{x} \right)^\lambda \frac{Q_0^2}{Q^2 + 4m_f^2} + 1 \right] + \left( \frac{x_0}{x} \right)^\lambda \frac{Q_0^2}{Q^2 + 4m_f^2} \times \ln \left[ \left( \frac{x}{x_0} \right)^\lambda \frac{Q^2 + 4m_f^2}{Q_0^2} + 1 \right] \right\}, \quad (21)$$

where the fixed parameters in this relation determined in Ref.[24] by fitting to small  $x$  experimental data of the proton structure function. Indeed Eq. (21) become to massless structure function when  $m_f$  sets to light quarks ( $m_f = 0.140$  GeV), and become to massive structure function when  $m_f \rightarrow m_Q$ .

In a convenient model [26], the cross-section of  $\gamma^*p$  scattering as function of the scaling variable  $\tau = Q^2/Q_s^2$  is proposed. A single universal curve, suggested by N. Armesto, C. Salgado, and U.A. Wiedemann [27], in what follows referred to as the ASW model (ASWM), describes the available experimental data on  $\sigma^{\gamma^*p}$  by the following form

$$\sigma^{\gamma^*p}(x, Q^2) \equiv \Phi(\tau) = \bar{\sigma}_0 [\gamma_E + \Gamma(0, \xi) + \ln \xi] \quad (22)$$

where  $\gamma_E$  and  $\Gamma(0, \xi)$  are the Euler constant and the incomplete  $\Gamma$  function, respectively. Authors in Ref.[27] extracted the  $\xi$  function from a fit to lepton-proton data as  $\xi = a/\tau^b$  with  $a = 1.868$  and  $b = 0.746$  for massless flavors. Therefore the proton structure function in ASW model reads

$$F_2^{ASW}(x, Q^2) = \frac{Q^2}{4\pi^2\alpha} \bar{\sigma}_0 \left[ \gamma_E + \Gamma(0, \xi) + \ln \xi \right]. \quad (23)$$

The ASW structure function (i.e., Eq.23) is considered in saturation physics.

#### 4. Heavy quarks structure functions

The standard parameterization of the singlet and gluon distribution functions with assuming the Regge-like behavior at small  $x$  is given by [28]

$$\begin{aligned} F_2^s(x, Q^2)_{x \rightarrow 0} &= x^{-\delta} \tilde{s}(x, Q^2), \\ x f_g(x, Q^2)_{x \rightarrow 0} &= x^{-\delta} \tilde{g}(x, Q^2). \end{aligned} \quad (24)$$

The Regge-like behavior of the distribution functions was proposed by Lopez and Yndurain [29]. The inclusive electroproduction on a proton was studied at low  $x$  and low  $Q^2$  using a soft and hard Pomeron in Ref.[30]. The value obtained by fixed coupling LLx BFKL gives  $\delta \simeq 0.5$ , which is the so-called hard-Pomeron exponent. Some other phenomenological models have also been proposed for the

singlet structure function exponent in Refs.[10] and [31]. In Ref.[32] authors presented a tensor-Pomeron model where it is applied to low- $x$  deep inelastic lepton-nucleon scattering and photoproduction processes. In this model, in addition to the soft tensor Pomeron, a hard tensor Pomeron and Reggeon exchange included. An effective behavior for the singlet structure function is reported in Refs.[10] and [33]. This effective exponent was found to be independent of  $x$  and to increase linearly with  $\ln Q^2$ . In Ref.[34] the CTEQ6.6C4 parametrization, which has a strong sea-like intrinsic charm contribution, give the  $\delta$  value that is the closet to 0.3 found in data and leads to a much better quality factor (QF) than the other parametrizations (as reported in Ref.[15]). For the behavior of the distribution functions and saturation scale, we use the GBW parametrization [11] with  $\delta = 0.288$ . This exponent of the saturation scale is known at next-to-leading order [35] and agrees with the values extracted from fits to new combined data.

Now exploiting the low  $x$  asymptotic behavior of  $f_{s,g}(x, Q^2)$  according to Eq.(24). We obtain the following equations for the  $Q^2$  derivative of the structure function (i.e., Eq.(14)) and heavy quark structure functions (i.e., Eq.(11)) by the following forms

$$\begin{aligned} \frac{\partial F_2(x, Q^2)}{\partial \ln Q^2} &= -\frac{1}{2} [r_{ss}(x, a_s, \delta) F_2(x, Q^2) \\ &\quad + \langle e^2 \rangle r_{sg}(x, a_s, \delta) x f_g(x, Q^2)], \\ F_k^{Q\bar{Q}}(x, Q^2) &= r_{k,g}(x, a_s, \delta) x f_g(x, Q^2), \end{aligned} \quad (25)$$

where

$$\begin{aligned} r_{ab}(x, a_s, \delta) &= \sum_{n=0} \tilde{P}_{ab}^{(n)}(x, a_s) \odot x^\delta, \\ r_{k,g}(x, a_s, \delta) &= \sum_{n=0} C_{k,g}^{(n)}(x, a_s) \odot x^\delta, \end{aligned}$$

where  $r$ 's is defined due to the splitting and Wilson coefficient functions. The convolution form  $A(x) \odot B(x)$  reads to be [36]

$$A(x) \odot B(x) \equiv \int \frac{dz}{z} A(a_s, z) B(z).$$

From Eqs.(25) one can obtain the heavy quark structure functions as a function of  $F_2$  and the derivative as

$$\begin{aligned} F_k^{Q\bar{Q}}(x, Q^2) &= -\frac{1}{\langle e^2 \rangle} \frac{r_{k,g}(x, a_s, \delta)}{r_{sg}(x, a_s, \delta)} \left[ 2 \frac{\partial F_2(x, Q^2)}{\partial \ln Q^2} \right. \\ &\quad \left. + r_{ss}(x, a_s, \delta) F_2(x, Q^2) \right]. \end{aligned} \quad (26)$$

Using the coefficient functions in the NNLO approximation for concrete value of  $\delta = 0.288$  we obtain an analytical equation for the heavy quark structure functions from above formulae (26) in the arguments of the function  $F_2$  and its derivative due to the BDH and ASW models.

A particular interests present the ratio of the longitudinal to transversal heavy quark structure functions, defined as

$$R^{\mathcal{Q}\overline{\mathcal{Q}}}(x, Q^2) = \frac{F_L^{\mathcal{Q}\overline{\mathcal{Q}}}(x, Q^2)}{F_2^{\mathcal{Q}\overline{\mathcal{Q}}}(x, Q^2)} = \frac{r_{L,g}(x, a_s, \delta)}{r_{2,g}(x, a_s, \delta)}. \quad (27)$$

In fact the proton structure function and its derivative cancel in the ratio of heavy quark structure functions, which is very useful for practical applications.

#### 4. RESULTS

With help of Eqs.(26) and (27) we have extracted the heavy quark structure functions and the ratio  $R^{\mathcal{Q}\overline{\mathcal{Q}}}$  from the parametrizations of the proton structure functions (i.e., BDH and ASW models) respectively. As for our input parameters, we choose the running charm and bottom quark masses  $m_c = 1.29^{+0.077}_{-0.053}$  GeV and  $m_b = 4.049^{+0.138}_{-0.118}$  GeV, where the uncertainties are obtained through adding the experimental fit, model and parameterization uncertainties in quadrature [7]. The strong coupling constant value is chosen to be  $\alpha_s(M_z^2) = 0.118$ . We employ the standard representation for QCD coupling and the coefficient functions in the NNLO approximation. To investigate GS for heavy quark structure functions we shall compare results obtained using scaling variable  $\tau$  (8). The parameters  $Q_0$  and  $x_0$  are related to the GBW model by  $Q_0 = 1$  GeV and  $x_0 = 3.04 \times 10^{-4}$ . Let us now confront the implications of geometrical scaling with our results and experimental data on heavy quark structure functions at low  $x$ . We have calculated the  $\tau$ -dependence, at low  $x$ , of the heavy quark structure functions  $F_2^{\mathcal{Q}\overline{\mathcal{Q}}}(\tau)/\tau$  with respect to the parametrization of  $F_2^{\text{BDH}}$  and  $F_2^{\text{ASW}}$  as described above, in the NNLO approximation, Eq. (26). Results of calculations and comparison with HERA data [16] for charm and bottom structure functions are presented in Figs.1 and 2, where the circles correspond to the extracted charm and bottom structure functions due to the BDH and ASW models in the NNLO approximation, respectively.

Figures 1 and 2 clearly demonstrate that the extraction procedures provide correct behaviors of the extracted heavy quark structure functions in both models at small  $\tau$ . At large  $\tau$  the extracted heavy quark structure functions due to the BDHM are in a good agreement with experimental data. This is visible as the ASWM has good agreement with the proton structure function for  $\tau < 100$  [26]. The deviation between these curves therefore shows the effect of the heavy quarks masses. In Figs.1 and 2 we show results for  $F_2^{c\overline{c}}(\tau)/\tau$  and  $F_2^{b\overline{b}}(\tau)/\tau$  as a function of the scaling variable  $\tau$  for different  $Q^2$  above 5 GeV<sup>2</sup> and  $x \geq 0.0002$  due to the data of the H1-Collaboration [16] and for 6.5 GeV<sup>2</sup> and  $x \geq 0.00015$  due to the data of the ZEUS-Collaboration [16]. The theoretical results

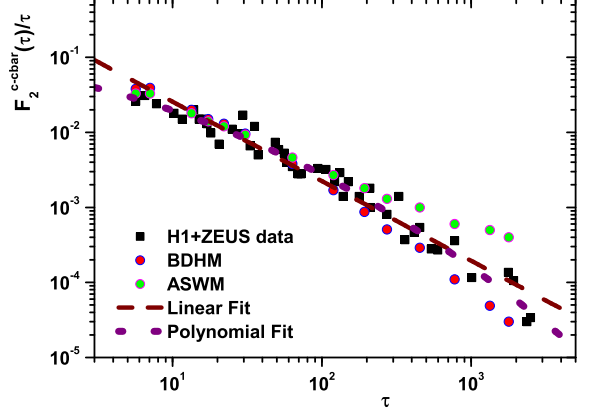


FIG. 1:  $F_2^{c\overline{c}}(\tau)/\tau$  as a function of scaling variable  $\tau$  with  $m_c = 1.29$ . Two circles correspond to proton structure functions due to the BDH and ASW models. Experimental data on the charm structure functions from the region  $x < 0.1$  collected corresponding to the H1 2010 and ZEUS 2014 data [16]. The linear (dashed curve) and non-linear (dotted curve) fits plotted in comparison with the HERA data.

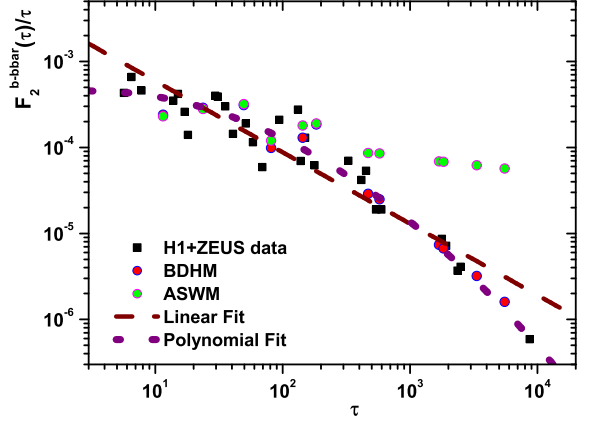


FIG. 2:  $F_2^{b\overline{b}}(\tau)/\tau$  as a function of scaling variable  $\tau$  with  $m_b = 4.049$ . Two circles correspond to proton structure functions due to the BDH and ASW models. Experimental data on the bottom structure functions from the region  $x < 0.1$  collected corresponding to the H1 2010 and ZEUS 2014 data [16]. The linear (dashed curve) and non-linear (dotted curve) fits plotted in comparison with the HERA data.

are presented for the same kinematical variables as the experimental data for average of the Bjorken values of  $x$ , and we see that there are good agreements between BDH theory and data at small and large  $\tau$ .

In Fig.1 we see that data exhibit GS over a very broad

region of  $\tau$ . We can clearly see that the charm structure functions reflects the fact that  $F_2^{c\bar{c}}(\tau)/\tau$  scales as  $1/\tau$ . The linear fit shows this scaling with a good accuracy. However a second-order polynomial fit shows that the change of shape of the dependence of  $F_2^{c\bar{c}}(\tau)/\tau$  on  $\tau$  from the approximate  $1/\tau$  dependence at large  $\tau$  to the less steep dependence at small  $\tau$  [8,37]. Important result is that the linear and non-linear fits to the charm structure functions exhibits GS by the following forms

$$\begin{aligned} F_2^{c\bar{c}}(\tau)|_{\text{Non-Linear}} &\simeq 0.06 \tau^{0.69} \exp[-0.08 \ln^2(\tau)], \\ F_2^{c\bar{c}}(\tau)|_{\text{Linear}} &\simeq 0.30 \tau^{-0.06}. \end{aligned} \quad (28)$$

The difference between linear and non-linear curves therefore represents the effect of saturation. From Fig.2 one can infer that the non-linear results essentially improve the agreement with data in comparison with the linear fit. We see that the experimental data are very well reproduced by the non-linear fits for bottom structure functions, which gives the behavior of  $F_2^{b\bar{b}}(\tau)/\tau$  on  $\tau$  from the asymptotic  $1/\tau$  dependence at large  $\tau$  to the less steep dependence at small  $\tau$ , which corresponds to the fact that at small values of  $\tau$  the bottom structure function grows weaker with energy than  $Q_s^2(x)$ . The linear and non-linear fits to the bottom structure functions are given by

$$\begin{aligned} F_2^{b\bar{b}}(\tau)|_{\text{Non-Linear}} &\simeq 0.0004 \tau^{1.2300} \exp[-0.1040 \ln^2(\tau)], \\ F_2^{b\bar{b}}(\tau)|_{\text{Linear}} &\simeq 0.004 \tau^{0.172}. \end{aligned} \quad (29)$$

In Figs.(3) and (4) we also found a symmetry between the regions of large and small  $\tau$  for the heavy quark structure functions due to the non-linear fits in comparison with the HERA data [16]. Figs.(3) and (4) indicate the present of symmetry of  $F_2^{c\bar{c}}$  and  $F_2^{b\bar{b}}$  in comparison with the HERA data [16] with respect to the transformation  $\tau \leftrightarrow 1/\tau$  in a wide range of  $\tau$  values [38]. With respect to Figs.(3) and (4), we also found a symmetry line between the regions of large and small  $\tau$  for the charm and bottom structure functions, which corresponds to the ratio of heavy quarks masses,  $m_b/m_c \simeq 3.139$ . The argument in symmetry line is  $\tau_b \simeq 3.139 \tau_c$ . In conclusion the features present in the average of the charm and bottom structure function can be well reproduced in the phenomenological saturation model as shown in (28) and (29), corresponding to the non-linear dashed curves in Figs.3 and 4. In Fig.5 we show comparison of the heavy quark structure functions,  $F_2^{c\bar{c}}/F_2^{b\bar{b}}$ , obtained using the non-linear behaviors for  $x = 10^{-2} \dots 10^{-5}$ . The ratio of the heavy quarks structure function increase as  $x$  decreases at low  $Q^2$ . It is clear that at low  $Q^2$  values the FFNS approach is valid. Here heavy flavors are not considered as active and are generated only by boson-gluon fusion (BGF). The charm and bottom quarks are infinity massive for  $Q^2 \leq m_Q^2$  and are massless above this threshold. For  $Q^2 \gg m_Q^2$  NNLO terms in the coefficient functions are enhanced by powers

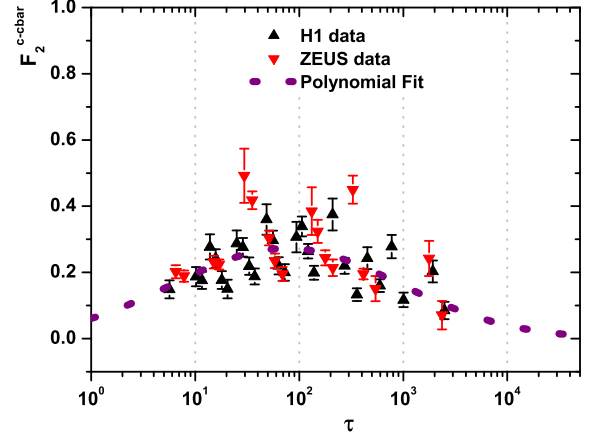


FIG. 3: The non-linear fits to the charm structure functions  $F_2^{c\bar{c}}(\tau)$  plotted versus the scaling variable  $\tau$ . Experimental data are from the H1 and ZEUS Collaborations, Ref.[16] as accompanied with total errors.

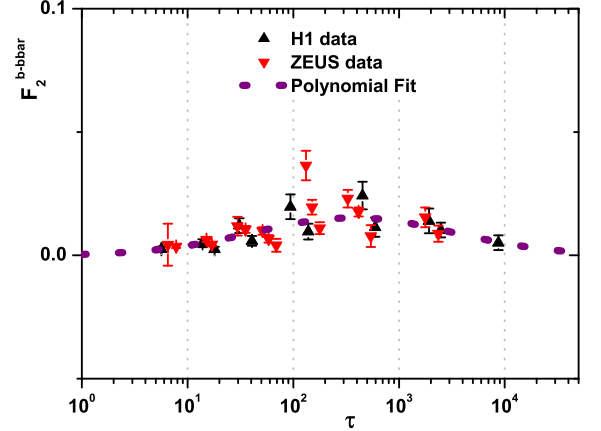


FIG. 4: The non-linear fits to the bottom structure functions  $F_2^{b\bar{b}}(\tau)$  plotted versus the scaling variable  $\tau$ . Experimental data are from the H1 and ZEUS Collaborations, Ref.[16] as accompanied with total errors.

of  $\log(Q^2)/m_Q^2$  where VFNS is valid in this region [15]. As we observe in Fig.5, this ratio is expected to rise for a given  $Q^2$  with decreasing  $x$  and fall for a given  $x$  with increasing  $Q^2$ , respectively. Indeed the ratio  $F_2^{c\bar{c}}/F_2^{b\bar{b}}$  at large  $Q^2$  is almost constant as for  $Q^2 = 10^4 \text{ GeV}^2$  the ratio is independent of the  $x$  variable (illustrated in right-hand side of Fig.5). In Figs.6 and 7 we investigated the ratio  $F_2^{c\bar{c}}/F_2^{BDHM}$  and  $F_2^{b\bar{b}}/F_2^{BDHM}$  whose behavior is very interesting in the range of available HERA energy [39,40] and its extension to future energies in LHeC and

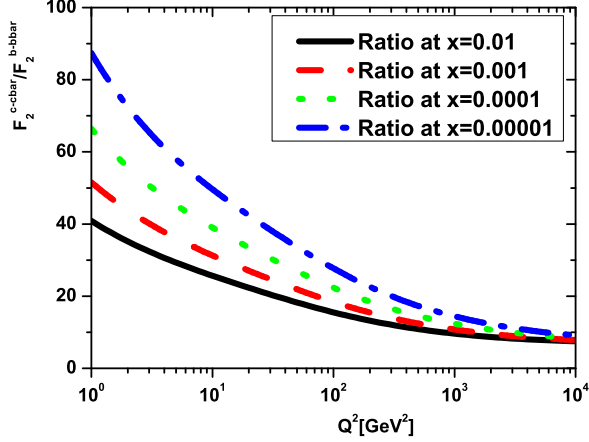


FIG. 5:  $F_2^{c\bar{c}}/F_2^{b\bar{b}}$  for fixed  $x$  as a function of  $Q^2$ .

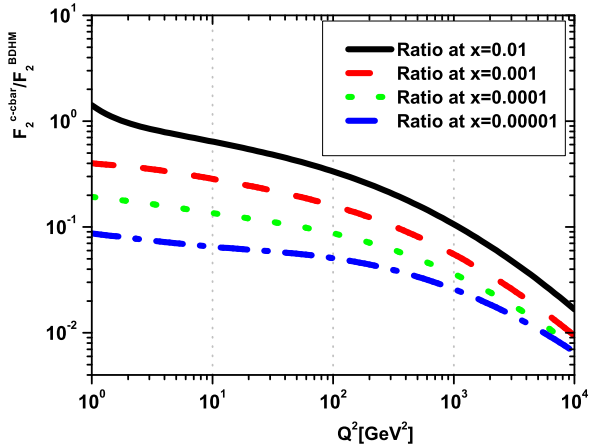


FIG. 6: The ratio  $F_2^{c\bar{c}}/F_2^{BDHM}$  is extracted from the charm non-linear structure function (i.e., Eq.28) and the parametrization of the proton structure function (i.e., Eq.15), in a wide range of  $Q^2$  for  $x = 10^{-2} \dots 10^{-5}$ .

FCC-eh [1]. In these figures (i.e., Figs.6 and 7) we shown the ratio of the heavy quarks structure functions where the  $F_2(x, Q^2)$  parameterization is taken from Ref.[22]. It is interesting that the values of these ratios are constant due to the HERA data range. HERA data range on the cross sections for the open charm and bottom production in neutral current deep inelastic electron-proton scattering (DIS) extended from  $Q^2 \sim \mathcal{O}(5 \text{ GeV}^2)$  and  $x \sim 10^{-4}$  until  $Q^2 \sim \mathcal{O}(1000 \text{ GeV}^2)$  and  $x \sim 10^{-2}$ . Therefore in Fig.6 we observe that the ratio  $F_2^{c\bar{c}}/F_2^{BDHM}$  is approximately between  $\sim 0.2 - 0.1$  as this prediction is close to the average result  $\langle F_2^{c\bar{c}}/F_2 \rangle = 0.237 \pm 0.021 \pm 0.041$ , in

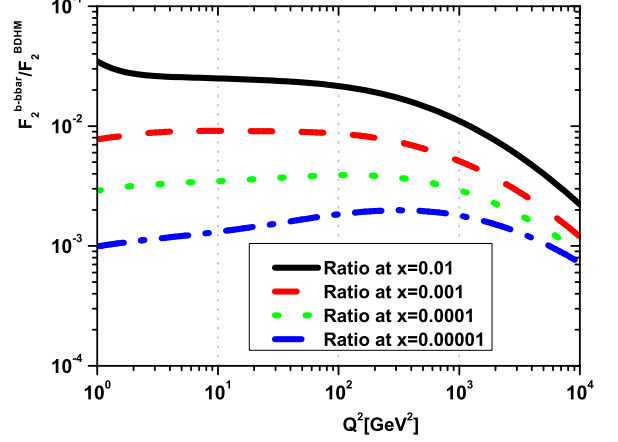


FIG. 7: The ratio  $F_2^{b\bar{b}}/F_2^{BDHM}$  is extracted from the bottom non-linear structure function (i.e., Eq.29) and the parametrization of the proton structure function (i.e., Eq.15), in a wide range of  $Q^2$  for  $x = 10^{-2} \dots 10^{-5}$ .

Ref.[39] and it is compatible with the measured results by EMC. In Fig.7 the ratio  $F_2^{b\bar{b}}/F_2^{BDHM}$  with respect to the HERA region is approximately between  $\sim 0.003 - 0.01$ . It is interesting that with increasing  $x$  and  $Q^2$  according to the HERA region, the ratio  $F_2^{c\bar{c}}/F_2^{BDHM}$  decreases while the ratio  $F_2^{b\bar{b}}/F_2^{BDHM}$  increases. These results in a wide range of  $x$  and  $Q^2$  can be applied as well in analyses of ultrahigh energy processes with cosmic neutrinos and will be able to be considered in the LHeC and FCC-eh collisions. In Figs.8 and 9 the photon-proton cross sections for charm and bottom production are shown, as  $\sigma^{c\bar{c}} \sim F_2^{c\bar{c}}/Q^2$  and  $\sigma^{b\bar{b}} \sim F_2^{b\bar{b}}/Q^2$ . In these figures we tested the properties of  $F_2^{Q\bar{Q}}/Q^2$  using the parameterization of the heavy-quark structure functions in a wide range of  $x$  and  $Q^2$ . The scaling properties of these functions as a function of the scaling variable  $\tau$  are shown in Figs.1 and 2. Geometrical scaling in heavy-quarks production should predominantly be regarded as a remarkable regularity of the inclusive DIS. In Fig.10 we show the  $\tau$  dependence of  $R^c(\tau)$  evaluated at NNLO approximation from Eq.(27) at  $\langle \mu^2 \rangle = Q^2 + 2m_c^2$ . Our calculations in the conventional (collinear) QCD factorization leads to more or less flat (independent on  $\tau$ ) behavior of  $R^c(\tau)$  with  $0.1 \lesssim R^c(\tau) < 0.2$  in a wide range of  $\tau$ . The results obtained are compatible with the collinear results in DAS approach and the TMD results at low  $Q^2$ . In Refs.[40-45] the results for the ratio of heavy quarks structure functions, obtained using the power-like behavior  $x^{-\delta}$ , can be found. Our calculations show that the collinear DAS predictions rather close to the results obtained due to the geometrical scaling at NNLO approximation. Indeed, the NNLO results obtained in the collinear perturbation the-



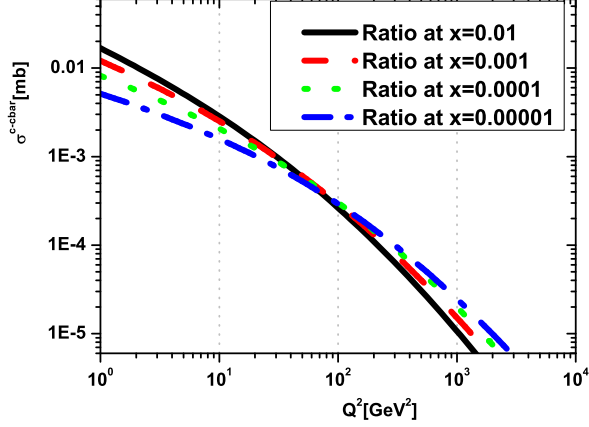


FIG. 8: The charm component  $\sigma^{c\bar{c}} \sim F_2^{c\bar{c}}/Q^2$  in a wide range of  $Q^2$  for  $x = 10^{-2} \dots 10^{-5}$ .

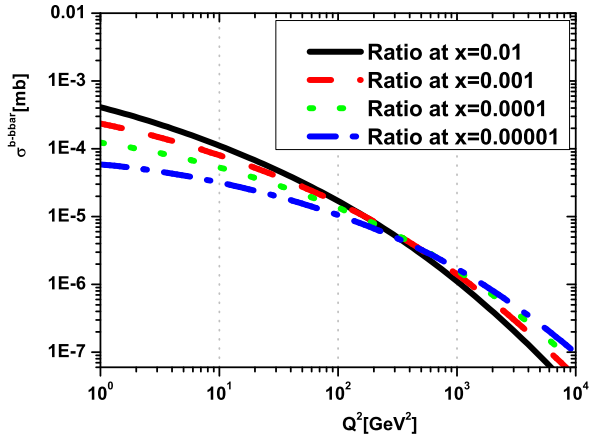


FIG. 9: The bottom component  $\sigma^{b\bar{b}} \sim F_2^{b\bar{b}}/Q^2$  in a wide range of  $Q^2$  for  $x = 10^{-2} \dots 10^{-5}$ .

ory due to the geometrical scaling lead to small values for the ratio  $R^c(\tau)$  in comparison with the corresponding  $Q^2$ -dependence evaluated with the TMD gluons. In fact, in collinear perturbation theory the ratio  $R^c(\tau)$  grow slowly when  $\tau$  increased.

## 5. CONCLUSIONS

We have shown that the charm and bottom structure function data exhibit geometrical scaling at low  $x$  in a wide range of  $Q^2$ , where  $F_2^{Q\bar{Q}}(\tau)/\tau$  is the function of only one dimensionless variable  $\tau = Q^2/Q_{sat}^2(x)$  with taking into account charm and bottom masses. We have

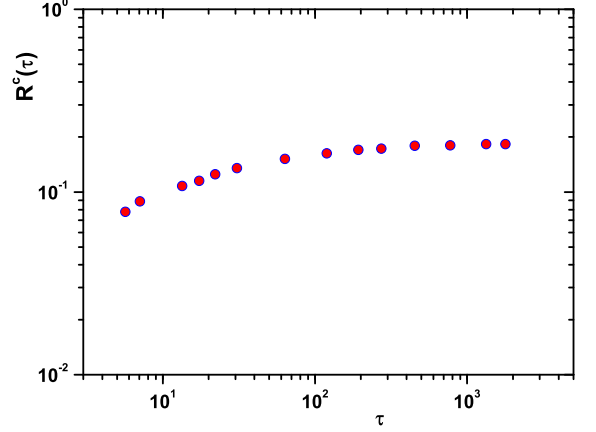


FIG. 10: The ratio of the charm structure function  $R^c(\tau)$  as a function of  $\tau$ .

used data from the HERA experiment [16]. Results obtained there suggest that polynomial fits predict the geometrical scaling of the charm and bottom structure function with a good accuracy. At low  $\tau$ , geometrical scaling may provide genuine evidence for parton saturation. We see the heavy quark structure functions exhibit geometric scaling for the whole  $Q^2$  range, verifying a transition in the behavior on  $\tau$  of the heavy quark structure functions from a smooth dependence at small  $\tau$  and an approximated  $1/\tau$  behavior at large  $\tau$ . The transition point between the charm and bottom structure functions is placed at  $\langle \mu^2 \rangle$ , which takes values of order  $m_b/m_c$  for a charm and bottom masses  $m_c = 1.290$  GeV and  $m_b = 4.049$  GeV respectively, and found a symmetry between the regions of large and small  $\tau$  for the charm and bottom structure functions with respect to the transformation  $\tau \leftrightarrow 1/\tau$  in the whole region of  $\tau$ .

In fact we have presented Eq.(26) for the extraction of the heavy quark structure function  $F_2^{Q\bar{Q}}$  at low  $x$  from the  $F_2$  and its  $\ln Q^2$  derivative with the explicit form of the proton structure function by the BDH and ASW parametrizations using the DAS approach at NNLO approximation. Moreover, we obtained the results for  $F_2^{c\bar{c}}/F_2^{b\bar{b}}$ ,  $F_2^{c\bar{c}}/F_2^{BDHM}$  and  $F_2^{b\bar{b}}/F_2^{BDHM}$  where they are seems to be extremely important for future colliders. Concerning the ratio  $R^c(\tau) \equiv F_L^{c\bar{c}}/F_2^{c\bar{c}}$ , we show that the results are flat in a wide range of  $\tau$  and they are similar to the ones obtained beyond LO of  $k_T$ -factorization calculations at low  $\tau$  and of collinear perturbation theory at large  $\tau$ . In Ref.[18], the  $k_T$ -factorization predictions obtained using derived analytical expressions for TMD gluon density. Finally we have investigated the scaling properties of  $\sigma^{Q\bar{Q}} \sim F_2^{Q\bar{Q}}/Q^2$  with respect



the parametrization of heavy quark structure function at low  $x$ .

## ACKNOWLEDGMENTS

The author is thankful to the Razi University for financial support of this project.

## REFERENCES

1. LHeC Collaboration and FCC-he Study Group, P. Agostini et al., J. Phys. G: Nucl. Part. Phys. **48**, 110501(2021).
2. S. Alekhin, J.Blümlein and S. Moch, Phys.Rev.D **102**, 054014 (2020).
3. J.Blümlein et al., Nucl.Phys.B **755**, 272 (2006).
4. S. Alekhin, J.Blümlein and S. Moch, Phys. Rev. D **86**, 054009 (2012).
5. R.D. Ball et al. [NNPDF Collaboration], Nucl. Phys. B **855**, 153 (2012).
6. R.Thorne, Phys.Rev.D **86**, 074017 (2012).
7. H.Abramowicz et al., [H1 and ZEUS Collaboration], Eur.Phys.J.C **78**, 473 (2018).
8. A.M.Stasto, K.Golec-Biernat and J.Kwiecinski, Phys.Rev.Lett. **86**, 596 (2001).
9. F.Gaola and S.Forte, Phys.Rev.Lett. **101**, 022001 (2008).
10. M.Paraszalowicz and T.Stebel, JHEP **04**, 169 (2013); T.Stebel, Phys.Rev.D **88**, 014026 (2013).
11. K.Golec-Biernat and M.Wüsthoff, Phys.Rev.D **59**, 014017 (1998); Phys.Rev.D **60**, 114023 (1999).
12. J.Jalilian-Marian, A.Kovner, A.Leonidov and H.Weigert, Nucl.Phys.B **504**, 415 (1997); Phys.Rev.D **59**, 014014 (1999); E.Iancu, A.Leonidov and L.D.McLerran, Nucl.Phys.A **692**, 583 (2001); E.Ferreiro, E.Iancu, A.Leonidov and L.D.McLerran, Nucl.Phys.A **703**, 489 (2002).
13. L.D. McLerran and R. Venugopalan, Phys. Rev. D **49**, 2233 (1994); Phys. Rev. D **49**, 3352 (1994); A. Ayala, J. Jalilian-Marian, L.D. McLerran and R. Venugopalan, Phys.Rev.D **52**, 2935 (1995); Phys.Rev.D **53**, 458 (1996).
14. A. Morreale and F. Salazar, Universe **7**, 312 (2021).
15. G.Beuf, C.Royon and D.Salek, arXiv [hep-ph]:0810.5082; R.S.Thorne, 9805298.
16. F.D.Aaron et al., (H1 Collaboration), Eur.Phys.J.C **65**, 89 (2010); H.Abramowicz et al., [ZEUS Collaboration], JHEP09, 127(2014).
17. E. Laenen et al., Phys. Lett. B **291**, 325 (1992); S. Alekhin and S. Moch, Phys. Lett. B **699**, 345 (2011).
18. A.V.Kotikov, A.V.Lipatov and P.Zhang, Phys.Rev.D **104**, 054042 (2021).
19. M.Gluck, E.Reya and A.Vogt, Z.Phys.C **67**, 433 (1998); Eur.Phys.J.C **5**, 461 (1995).
20. A.Yu.Illarionov, B.A.Kniehl and A.V.Kotikov, Phys.Lett.B **663**, 66 (2008).
21. H.Kawamura, N.A.Lo Presti, S.Moch and A.Vogt, Nucl.Phys.B **864**, 399 (2012).
22. M. M. Block, L. Durand and P. Ha, Phys. Rev.D **89**, 094027 (2014).
23. L.P.Kaptari, A.V.Kotikov, N.Yu.Chernikova and Pengming Zhang, Phys.Rev.D **99**, 096019 (2019); G.R.Boroun and B.Rezaei, Phys.Rev.D **105**, 034002 (2022).
24. Y.Hu et al., Eur.Phys.J.A **51**, 159 (2015).
25. N.N.Nikolaev, B.G.Zakharov, Z.Phys.C **49**, 607 (1990).
26. N.Armento, C.Merino, G.Parente, E.Zas, Phys.Rev.D **77**, 013001 (2008).
27. N.Armento, C.Salgado, and U.A.Wiedemann, Phys.Rev.Lett. **94**, 022002 (2005); J.L.Albacete, N.Armento, J.G.Milhano, C.A.Salgado, and U.A.Wiedemann, Eur.Phys.J.C **43**, 353 (2005).
28. A.V.Kotikov, J.Exp.Theor.Phys. **80**, 979 (1995); A.V.Kotikov and G.Parente, Mod.Phys.Lett.A **12**, 963 (1997).
29. C.Lopez, F.J.Yndurain, Nucl.Phys.B **171**,231 (1980).
30. J.R.Cudell, A.Donnachie and P.V.Landshoff, Phys.Lett.B **448**, 281 (1999).
31. B.Rezaei, G.R.Boroun, Eur.Phys.J.A **55**, 66 (2019).
32. D.Britzger, et al., Phys.Rev.D **100**, 114007 (2019).
33. C.Adloff, et al., H1 Collaboration, Phys.Lett.B **520**, 183 (2001).
34. P.M.Nadolsky et al., Phys.Rev.D **78**, 013004 (2008).
35. D.N.Triantafyllopoulos, Nucl.Phys.B **648**, 293 (2003).
36. G.R.Boroun and B.Rezaei, Phys.Lett.B **816**, 136274 (2021).
37. E.Avsar and G.Gustafson, JHEP **04**, 067(2007).
38. V.P.Goncalves and M.V.T.Machado, Phys.Rev.Lett. **91**, 202002(2003).
39. K.Daum et al., arXiv [hep-ph]:9609478.
40. G.R.Boroun and B.Rezaei, EPL **133**, 61002 (2021).
41. N.N.Nikolaev, J.Speth and V.R.Zoller, Phys.Lett.B **473**, 157 (2000); N.N.Nikolaev and V.R.Zoller, Phys.Lett.B **509**, 283(2001); N.N.Nikolaev and V.R.Zoller, Phys.Atom.Nucl. **73**, 672(2010); R.Fiore, N.N.Nikolaev and V.R.Zoller, JETP Lett. **90**, 319 (2009).
42. G.R.Boroun and B.Rezaei, Int.J.Mod.Phys.E **24**, 1550063 (2015); Nucl.Phys.A **929**, 119 (2014); Nucl.Phys.B **857**, 143 (2012); EPL **100**, 41001 (2012).
43. N.Ya.Ivanov, Nucl.Phys.B **814**, 142 (2009).
44. G.R.Boroun, Chin.Phys.C **45**, 063105 (2021); Nucl.Phys.B **884**, 684 (2014).
45. A.Donnachie and P.V.Landshoff, Phys.Lett.B **470**, 243 (1999).